Extreme precipitation response to climate perturbations in an atmospheric mesoscale model

Jisk J Attema[1], **Jessica M Loriaux**[1,2] **and Geert Lenderink**[1]

[1] KNMI, Utrechtseweg 297, PO box 201, 3730 AE, de Bilt, The Netherlands
[2] Delft University of Technology, Stevinweg 1, PO-box 5048, 2600 GA, Delft, The Netherlands

E-mail: jiskattema@gmail.com

Abstract

Observations of extreme (sub-)hourly precipitation at mid-latitudes show a large dependency on the dew point temperature often close to 14% per degree—2 times the dependency of the specific humidity on dew point temperature which is given by the Clausius–Clapeyron (CC) relation. By simulating a selection of 11 cases over the Netherlands characterized by intense showers, we investigate this behavior in the non-hydrostatic weather prediction model Harmonie at a resolution of 2.5 km. These experiments are repeated using perturbations of the atmospheric profiles of temperature and humidity: (i) using an idealized approach with a 2° warmer (colder) atmosphere assuming constant relative humidity, and (ii) using changes in temperature and humidity derived from a long climate change simulation at 2° global warming. All perturbations have a difference in the local dew point temperature compared to the reference of approximately 2°. Differences are considerable between the cases, with dependencies ranging from almost zero to an increase of 18% per degree rise of the dew point temperature. On average however, we find an increase of extreme precipitation intensity of 11% per degree for the idealized perturbation, and 9% per degree for the climate change perturbation. For the most extreme events these dependencies appear to approach a rate of 11–14% per degree, in closer agreement with the observed relation.

S Online supplementary data available from stacks.iop.org/ERL/9/014003/mmedia

1. Introduction

Events of extreme precipitation have a large impact on society, as they can cause flooding, disruption of infrastructure, erosion, agricultural crop damage and even loss of life. Ample studies claim that an increase in the frequency of the extreme precipitation events is to be expected in a warming climate, which is already apparent from present-day trends (e.g. Min *et al* 2011). Precipitation is determined to a large extent by

available energy and moisture (Held and Soden 2006, Muller and O'Gorman 2011). Energy constraints are expected to result in an increase in global mean precipitation of 1–3% per degree temperature rise (Allen and Ingram 2002, Held and Soden 2006). However, extreme precipitation is assumed to be constrained by the moisture availability, which will generally rise in a warming climate, roughly following the saturation specific humidity of the atmosphere (O'Gorman and Muller 2010). The latter is governed by the Clausius–Clapeyron (hereafter CC) equation, which gives a increase of 6–7% per degree temperature rise. It has been suggested that precipitation extremes should follow the same rate of increase of

6–7% per degree (Allen and Ingram 2002, Pall *et al* 2006), which we shall refer to as CC scaling. Others argue that changes in the lapse rate of the atmosphere and vertical velocities could cause deviations from CC scaling (O'Gorman and Schneider 2009a, Trenberth *et al* 2003, Sugiyama *et al* 2010).

Global climate models do show an increase of heavy precipitation with temperature for daily precipitation extremes. An analysis of the models participating in the IPCC AR4 and AR5 shows an average scaling of 5–6% per degree global warming, with the majority of the models falling between 4% and 10% per degree (Kharin *et al* 2007, 2013). For the tropics, however, O'Gorman (2012) finds a very large spread in the scaling of global climate models between almost zero and 30% per degree. The large spread is linked to the response of vertical motions in the atmosphere to climate change (O'Gorman and Schneider 2009b): Using observational constraints, however, his best estimate is 10% per degree, with a uncertainty range of 6–14% per degree. While deep convection plays a key role in the tropical climate, the dynamics of convective showers are not resolved in climate models and relatively simple parameterizations are used. It is often argued that the parameterizations and their interaction with the resolved dynamics are responsible for most of the uncertainty discussed above.

In this letter we will focus on small spatial (local) and short time (hourly) scales which are likely to be affected by convective precipitation. A part of the discrepancy between our results and the aforementioned GCM results could therefore be related to differences in scale and the atmospheric processes acting on these different scales.

Based on observations over western Europe, Lenderink and van Meijgaard find a temperature dependency of hourly precipitation extremes of approximately twice the CC relation for temperatures above 12 °C (Lenderink and van Meijgaard 2008, 2010). We will refer to this enhanced scaling compared to the CC relation as super-CC scaling. Lenderink *et al* (2011) also established for data from the Netherlands a clear link between this relation derived from day-to-day variations and the long term climate variations in hourly precipitation extremes over the last century.

It has been proposed that the origin of the super-CC scaling is a statistical one (Haerter and Berg 2009). However, a number of recent studies add evidence to the hypothesis that the super-CC scaling is a property of convective precipitation. For example, Berg *et al* (2013) explicitly use observations of cloud type to discriminate between convective and large scale precipitation, and find super-CC scaling for convective precipitation, whereas large scale precipitation follows CC scaling.

Indeed, looking at 10 min precipitation extremes from the Netherlands which are primarily determined by convective precipitation, Loriaux *et al* (2013) find twice CC scaling over an almost 20° temperature range. This range is much larger than the temperature range for which twice CC scaling is obtained in hourly precipitation. Loriaux *et al* (2013) also study the mechanism of the enhanced CC scaling with a simple 1D model for a convective plume, and find a dependency of

~10% per degree. However, this model does not resolve the three dimensional dynamics of convective clouds.

A small number of studies use a 3D cloud resolving model to research convective precipitation under warmer climate conditions. For the tropics, two studies find precipitation increases approximately consistent with CC scaling (Muller *et al* 2011, Muller 2013, Romps 2011). In these studies the atmosphere is allowed to react to future climate conditions through an equilibrium process. However, Muller *et al* (2011) use a higher sea surface temperature and let the system equilibrate to radiative convective equilibrium, whereas Romps (2011) uses a higher CO_2 concentration and a slab ocean model to obtain a future climate state.

For the mid-latitudes, evidence of super-CC scaling is found in a case study of an idealized squall line (Singleton and Toumi 2013). The setup differs from the two tropical studies mentioned above. Rather than allowing the system to evolve to an (quasi) equilibrium state, which mean values largely determined by energy constraints, Singleton and Toumi perturb the initial conditions and investigate the direct response of precipitation to these perturbations. The perturbation consists of a vertically uniform temperature perturbation, and atmospheric moisture is perturbed assuming unchanged relative humidity. In this setup the surface moisture therefore increases at a rate of 6–7% per degree.

Recent work has shown that the precipitation scaling might depend on how the atmospheric temperature is perturbed, with behavior closer to CC scaling if the atmosphere is perturbed according to a moist adiabat compared to super-CC scaling for a uniform temperature perturbation (Loriaux *et al* 2013). Such a moist adiabatic perturbation is considered more representative behavior for the tropics, whereas at mid-latitudes a vertically uniform temperature perturbation might be more appropriate. Also, changes in humidity aloft could influence the intensity of precipitation (Böing *et al* 2012).

In this study we extend the work of Singleton and Toumi in two ways. First, instead of one idealized case of convection, we study 11 cases characterized by intense (convective) precipitation in which realistic orography and surface interactions are included. These cases are based on observed weather situations. Second, besides using idealized perturbations, we also consider a more realistic perturbation that is obtained from a long simulation with a regional climate model. We will investigate how extremes in hourly precipitation depend on the change in near surface dew point temperature, which actually directly measures the near surface absolute humidity; a discussion on the use of dew point temperature is given in Section 2. While our main focus is on extremes in hourly precipitation, we will also consider instantaneous precipitation intensity and the size of the area with precipitation.

2. Methods

2.1. Model description

The case studies are performed using Harmonie version 37h1.1 (Bubnová *et al* 1995, Benard *et al* 2010, Seity *et al* 2011). Harmonie is a so-called convection permitting (i.e., the largest convective scales are explicitly resolved) atmospheric mesoscale

Table 1. The four experiments. A '—' indicates the field is unchanged with respect to the E_{ref} experiment. Here, *T* is the atmospheric temperature, RH the relative humidity, T_{surf} the land surface temperature, and SST the sea surface temperature.

Experiment	*T*	RH	T_{surf}	SST
E_{ref}	—	—	—	—
E_T^{min}	−2°C	—	−2°C	−2°C
E_T^{plus}	+2°C	—	+2°C	+2°C
E_C	Profile	Profile	+2.5°C	+2°C

model that is used in operational weather forecasting in a number of European countries (www.hirlam.org). The non-hydrostatic dynamical kernel is used in combination with Arome physics. For the surface we use a three layer ISBA surface scheme. The Harmonie domain contains 540 by 600 points at 2.5 km resolution, centered at 3.0° E and 53.0° N, with 60 levels in the vertical. A case runs from midnight to midnight, using a 1 min time step. Boundaries are updated every hour.

The model is nested in a hindcast using the KNMI Regional Atmospheric Climate Model version 2 (RACMO2) (van Meijgaard *et al* 2008), driven by ERA-Interim boundaries (Dee *et al* 2011), it starts at noon and runs for 36 h. Thus, RACMO2 is used to interpolate the coarser resolution of ERA-interim, 1.5° and 6 hourly fields, to 0.11° and hourly fields, respectively.

2.2. Experiment

A selection of 11 days characterized by intense precipitation is simulated over the Netherlands. For each day we construct four experiments by applying different perturbations to the temperature and humidity, see table 1. The perturbations are applied to the initial conditions of the runs (atmosphere and land) as well as the driving sea surface temperature, see the appendix for technical details. The four experiments consist of a reference case, E_{ref}, a homogeneous temperature shift of plus and minus 2 °C, E_T^{plus} and E_T^{min}, respectively, and a perturbation based on a climate change simulation, E_C.

In the idealized perturbations of plus and minus 2 °C independent of height, the relative humidity is unchanged with respect to the reference, based on evidence in literature (Colman 2004, Soden and Held 2006). This implies that the absolute surface humidity will increase with 6–7% per degree temperature rise.

In E_C a more realistic perturbation derived from an ensemble of climate change simulations is used, referenced shortly as the climate change perturbation. The output of an eight member ensemble of RACMO2 covering the period 1950–2100 is analyzed with respect to changes in the vertical profiles of the atmosphere over the Netherlands. This ensemble is forced by an ensemble of eight model runs with the global climate model EC-Earth (Hazeleger *et al* 2012). The model configuration of global model runs are identical to those performed for CMIP5 (Taylor *et al* 2012) and use the RCP8.5 greenhouse gas scenario. Differences between the 8 members

are caused by a small perturbation in the initial conditions of the global climate model runs at 1950. Profile data of the atmosphere is available at seven grid points of the regional climate model in the Netherlands, with a frequency of 1 h.

In order to determine the climate change perturbation, we compare the profile change between the reference period 1981–2010 and the future period 2046–2075 in which the 30-year average global mean temperature rise reaches 2 °C. Since all of the selected cases occur in the summer months, we only consider the summer season (JJA). The 30-year change in the profile of temperature and relative humidity, averaged over the 7 points in the Netherlands and over the day is shown in figure 1. The average temperature increase is slightly smaller than 2° (between 1.8 and 2 °C) from the surface up to a pressure level of 850 hPa. The temperature response gradually increases up to 3 °C at 300 hPa. Thus, the atmospheric temperature lapse rate slightly decreases in the climate change simulation. The relative humidity slightly decreases with 1–2% between the surface and 300 hPa, and increases by 5% near 200 hPa. We note that this result is in line with figure 2 in Sherwood *et al* (2010) for the Netherlands (latitude 52° N).

Since our cases are characterized by intense precipitation associated with strong convective activity, average profile changes may not be very representative. Therefore, a further selection is made based on CAPE (convective available potential energy), and the changes in these selected profiles are used for the climate perturbation.

The RACMO2 profiles of the 1000 hours with the highest CAPE values are averaged for each month, after which the resulting profiles of June, July and August are combined into one. The resulting profile for the reference period and the climate change signal derived from the difference between future and reference period are shown in red in figure 1. These profile changes are used for the E_C experiments. When we compare these to the constant temperature shift of the E_T^{plus} experiment we find that they have a larger temperature increase, especially in the lower atmosphere. The lower atmosphere also becomes dryer in relative terms, but the absolute humidity at the surface is comparable: a 2.5 °C temperature increase and a drop of relative humidity of about 5% at the surface results in an increase in dew point temperature of almost 2 °C.

We note that the stronger warming near the tropopause may well suggest a response of the atmosphere according to a moist adiabat—a response which is representative for the tropics. However, a moist adiabatic adjustment would imply a warming near the tropopause (at 200–300 hPa) of 3°–4° given the 2° increase in surface dew point; see Loriaux *et al* (2013) for details. For the profile change associated with the high CAPE situations the decrease in lapse rate due to the warming aloft is partly compensated by a stronger surface warming, associated with a reduction of relative a humidity. Therefore, the profile change is much closer to a constant temperature perturbation with height than to a temperature perturbation following a moist adiabat.

Finally, with the perturbations we aim to transpose the selected cases to plausible warmer (and colder) climate conditions. As these cases are all characterized by intense convective and therefore turbulent motions it is important that the
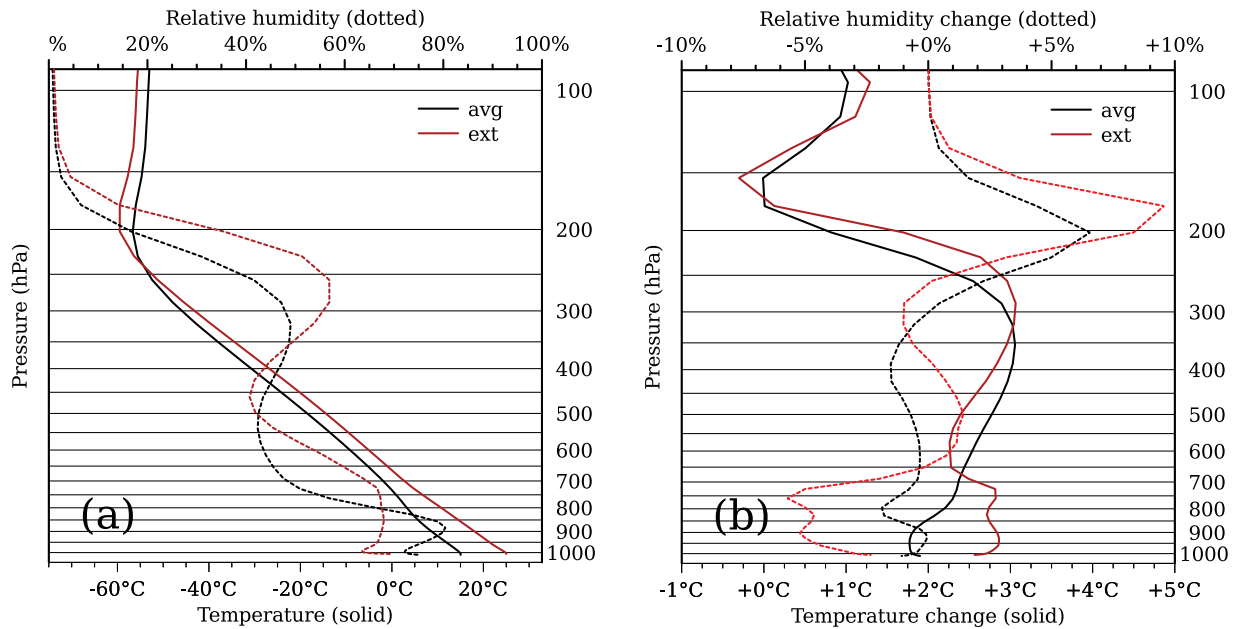
Figure 1. Atmospheric profiles for temperature (solid lines) and relative humidity (dashed lines) for the averaged atmosphere (black) and the average over the hours with highest CAPE (red). (a) for the present (1981–2010); (b) the changes in the near future (2046–2075), corresponding to 2 °C global temperature increase.

mesoscale dynamics and therefore convective cloud structures of these cases remain comparable. This way, unpredictable error growth of 3D turbulence doesn't inhibit a direct comparison between the cases. Inspection of the precipitation field shows that in general this condition is met. With the possible exception of case 10, the time evolution as well as the daily fields of precipitation remain very similar in the perturbed experiments compared to the reference experiment.

2.3. Analysis of the scaling

We use the local dew point temperature in our analysis for the following reasons. From the observations more robust results are generally obtained using the local dew point temperature instead of the local temperature; there is a wider range where the scaling is valid and a better consistency between different stations (Lenderink and van Meijgaard 2010, Lenderink *et al* 2011). Also the use of dew point temperature is physically more justified. It directly measures the absolute humidity of the air, which is relevant in this respect as it is the increase in humidity with global warming that underlies our confidence in the projected increase in precipitation extremes. Now, if the relative humidity does not change the increase in dew point temperature will be equal to the temperature increase. The assumption of constant relative humidity is reasonable for many areas and seasons, except for large continental areas in summer (Willett *et al* 2010). But as a matter of fact, the rise in dew point temperature is reasonably robust across Europe, and appears more robust than the rise in temperature; see supplementary material of Lenderink *et al* (2011). In the text we will rather loosely use temperature, but this refers to the local dew point temperature.

The increase in dew point temperature is 2° by construction in the E_T^{plus} experiment. It is slightly less than 2° (i.e.

1.9°) in the E_C experiment, and therefore almost equals the global mean temperature rise of 2° in the runs from which the perturbation is derived. For ease of computation we use 2° for both E_T^{plus} and E_C perturbations, noting that the difference in the results would be small (i.e. less then 1% in the obtained scaling factors α).

Since the relation between dew point temperature and moisture is approximately exponential, we look for an exponential increase in precipitation extremes with temperature. We call this 'scaling', and define the rate of increase as α,

$$P' = P\alpha^{\Delta T}. \qquad (1)$$

Here P is a percentile in the reference experiment E_{ref} and P' the same percentile in a perturbed experiment. By taking different pairs of experiments we can solve this for α:

$$\alpha_C = \sqrt{P_C/P_{ref}}, \qquad \alpha_T^{plus} = \sqrt{P_T^{plus}/P_{ref}},$$
$$\alpha_T^{min} = \sqrt{P_{ref}/P_T^{min}}, \qquad (2)$$

where α_T^{plus} and α_T^{min} are the rate of increase for a 2 °C temperature change assuming constant relative humidity, and α_C is the rate of increase under simulated climate change. Finally, α_T is calculated by a least-squares fit of equation (1) to the percentiles of the three experiments with the same relative humidity.

In our analysis we focus on a sub-region spanning from -1 to 10° E by 47.5 to 57° N. By pooling the hourly precipitation amounts for all grid points in this region for every hour, we are left with one dataset per experiment (containing 3.08 million points) from which the precipitation percentiles are determined. Scaling factors are calculated for each percentile independently. The separate scalings over the 99.9, 99.99, and 99.999 percentile are also averaged for quick comparison between the experiments.
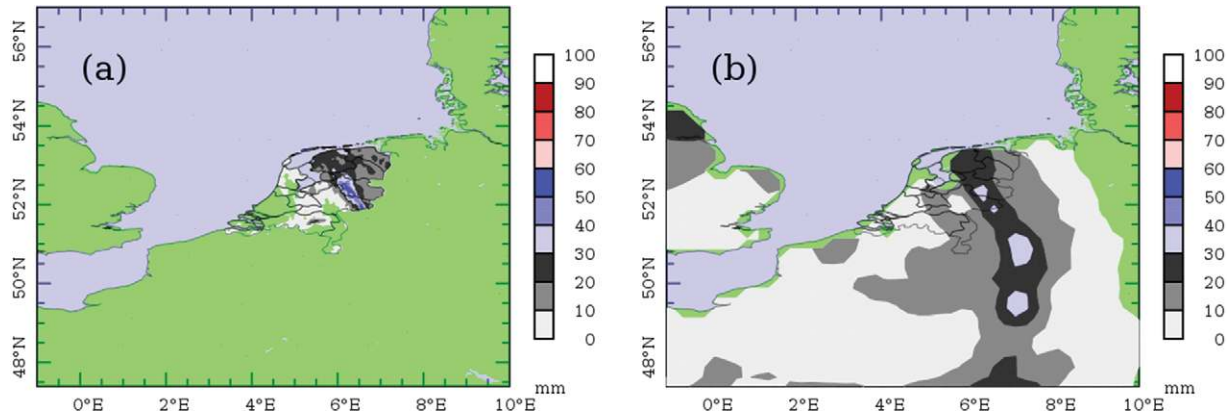
Figure 2. Case 6: August 11 2011. (a) Accumulated rain radar observations over the Netherlands; (b) Summed E-OBS data for August 10 and August 11. Background colors indicate land (green) or sea (light blue).

Table 2. Shower events analyzed in this letter, and the maximum of the 1-h accumulated precipitation (pr_{max}). Temperature, dew point temperature, and relative humidity are taken 2 m above the surface. They are averaged over the 9×9 grid points surrounding the precipitation maximum, 1 h before the maximum occurred.

Case	Date	pr_{max} (mm h^{-1})	T (°C)	T_d (°C)	RH (%)
1	3 September 1998	44	20	18	85
2	7 August 1999	54	20	18	86
3	3 August 2000	64	17	14	83
4	5 August 2001	42	15	12	84
5	5 August 2002	118	21	18	83
6	11 August 2004	67	21	19	90
7	19 August 2005	97	21	17	76
8	7 August 2008	57	20	18	91
9	13 July 2010	97	23	21	92
10	28 June 2011	44	27	16	50
11	18 August 2011	63	25	21	74

2.4. Cases

Using station observations of precipitation, lists compiled by amateur meteorologists, and considering societal impact, we made a selection of extreme summer precipitation events with a large convective component by a cursory check of the synoptic situation and of the weather forecast from the day before the event. The resulting 11 days are listed in table 2. While each case is one of heavy convective precipitation, the cases cover a wide range of synoptic situations. As a result, the meteorological conditions in the reference experiment taken just before the precipitation maximum span a wide range of precipitation intensities (42–118 mm h^{-1}), temperatures (15–27 °C), and dew point temperatures (12–21 °C).

3. A single case example

In order to illustrate a number of general features of the results, we first look at case 6 (August 11, 2011) in more detail. We focus on this particular case because the precipitation field has clearly defined structures, making it easier to identify the general features of the precipitation response to the perturbations. Note however, that this case has a relatively strong response to the perturbations compared to the full set of cases.

Case 6 consists of a band of precipitation which is caused by a shower crossing the Netherlands from the east to the north-west (figure 2(a)). Figure 2(b) shows the same event for the gridded observational data set E-OBS (Haylock *et al* 2008). Note that because this event is spread across two E-OBS accumulation intervals from 08:00 to 08:00, two days have been combined to visualize the event. The simulation of precipitation in Harmonie is shown in figure 3. Although the shower location has shifted a bit to the south-west, it verifies reasonably well with the observations considering that the weather model is nested in a regional climate model and no data assimilation was used. After all, it is not our purpose to reproduce the observations exactly, but merely to perform simulations of extreme precipitation under a range of atmospheric conditions.

Comparison of the four Harmonie simulations in figure 3 shows that the structure of the precipitation field remains very similar in the perturbed experiments with respect to the reference experiment. Apparently, there is no significant random component due to 3D turbulent motions that leads to incomparable results. As expected, the E_T^{plus} and E_C experiments display an increase in maximum precipitation amounts, while the negative temperature perturbation experiment, E_T^{min} shows a decrease in maximum precipitation. In addition, the climate perturbation causes the disappearance of some areas
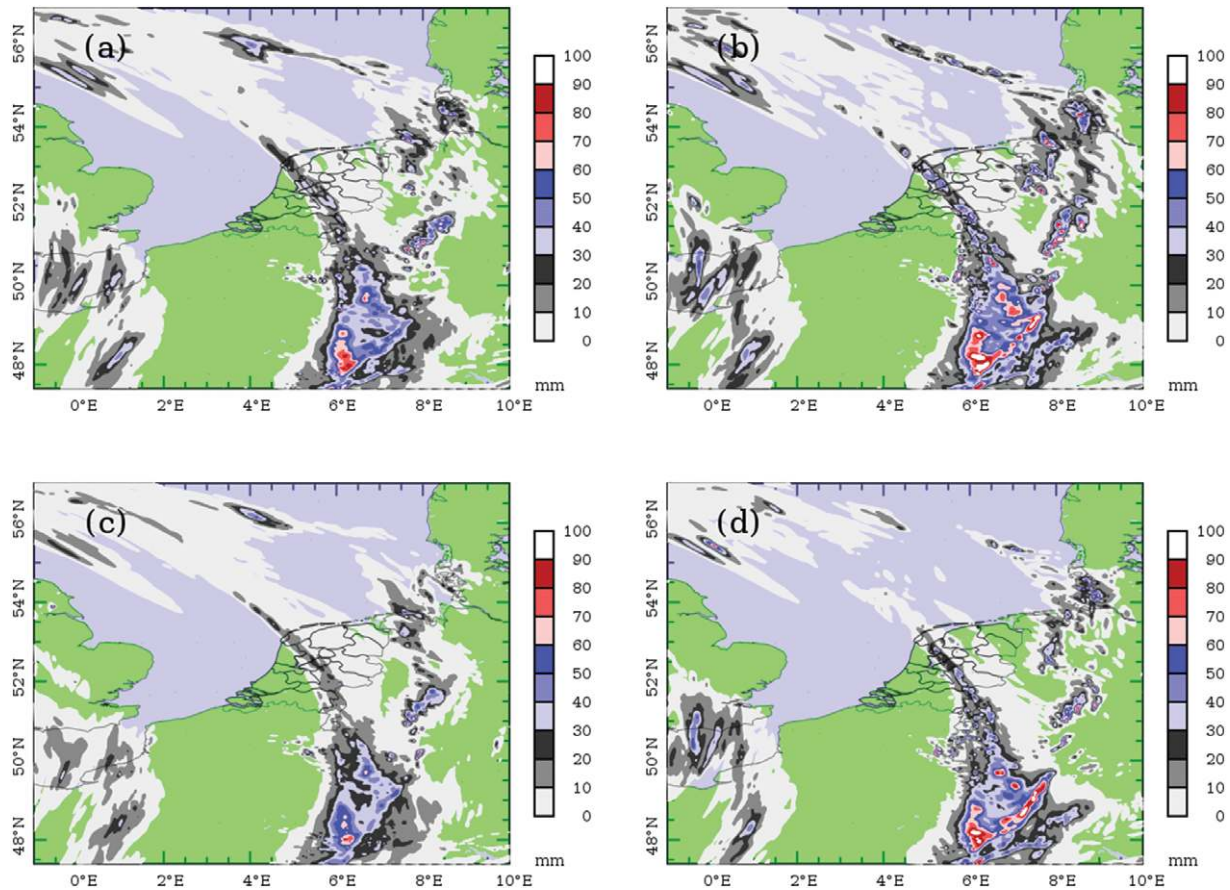
Figure 3. Total precipitation for case 6 for the 4 experiments: (a) E_{ref}; (b) E_T^{plus}; (c) E_T^{min}; (d) E_C.

with light rain in the reference simulation, for instance over the North Sea.

Figure 4 shows the time evolution of the event size during the day. The area is computed from hourly precipitation exceeding different thresholds of 1, 10 and 30 mm h^{-1}, respectively. The timing of the maxima in precipitating area remains similar under all perturbations, again confirming that the perturbations have little impact on the mesoscale dynamics. For the lowest threshold of 1 mm h^{-1}, the E_C experiment shows a reduction of the precipitating area with respect to E_{ref} which is most pronounced during the middle of the day. It is likely that this reduction is related to the decrease in relative humidity in this perturbation. The idealized perturbations show a small increase in event size with temperature of approximately 5% per degree temperature rise (see table B1 of the supplementary material available at stacks.iop.org/E RL/9/014003/mmedia). The area with intense precipitation (exceeding 30 mm h^{-1}) shows an increase for E_C, as well as for the idealized perturbations. This is in agreement with figure 3.

The probability of exceedance (POE) derived from pooling all hourly precipitation of all grid point and all hours during the day is shown in figure 5(a). We note that although we use the term 'percentiles', we plot the POE because for the higher percentiles the large number of 9's become unwieldy. For the highest percentiles a clear increase in intensity with
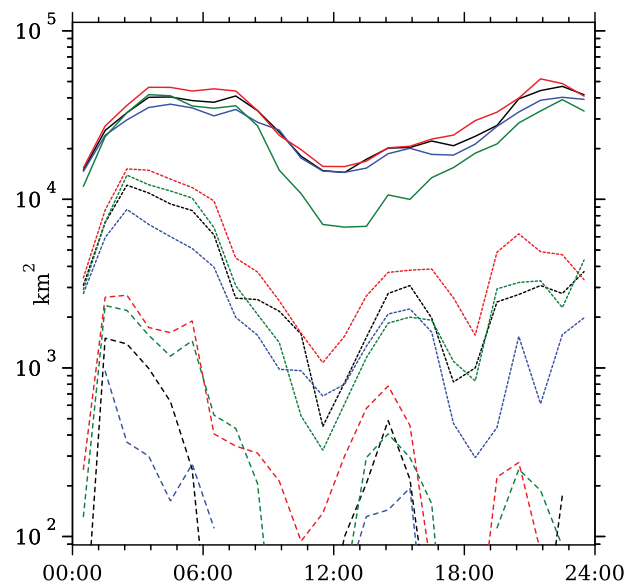

Figure 4. Case 6, Size of the precipitation event for a threshold of 1 (solid), 10 (dotted), and 30mm h^{-1} (dashed). Color indicates the experiment: E_{ref} (black), E_T^{plus} (red), E_T^{min} (blue), and E_C (green).

temperature can be seen, with considerably higher precipitation intensities for E_T^{plus} and E_C than the reference experiment. Similarly, the negative temperature perturbation experiment
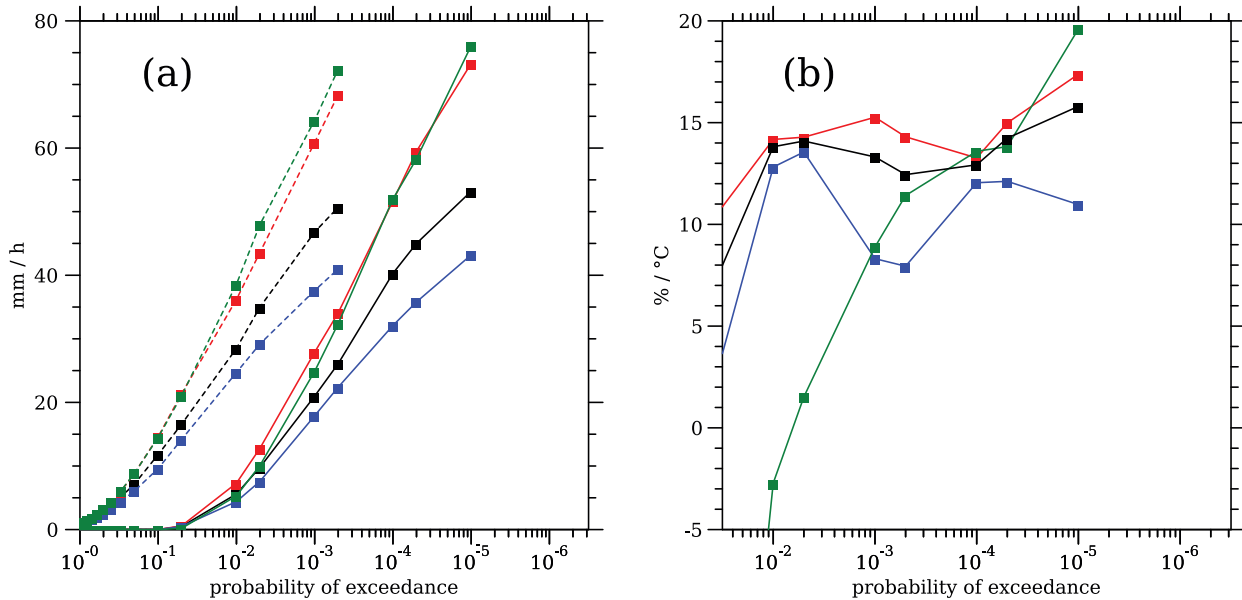
Figure 5. (a) The probability of exceedance for the 1-h precipitation intensities in mm h^{-1} for case 6. The different experiments are color coded: E_{ref} in black; E_T^{min} in blue; E_T^{plus} in red; E_C in green. Solid lines include all data while dotted lines include data conditioned on a cut-off of 1mm h^{-1}. (b) Precipitation scaling for α_T^{plus} (red), α_T^{min} (blue), α_T (black), and α_C (green).

shows lower intensities. The dotted lines in figure 5(a) represent the POE conditioned on precipitation amounts larger than 1 mm h^{-1}. Results of E_T^{plus} and E_C are similar for the lower percentiles, showing that the statistics of the lower percentiles are primarily affected by the change in the frequency (area extent) of precipitation.

Figure 5(b) shows the increase of precipitation intensity with temperature in terms of percentiles (we will refer to this as scaling). The scaling has been derived from sets of two or three experiments: α_T^{plus} from E_T^{plus} and E_{ref}; α_T^{min} from E_T^{min} and E_{ref}; α_T from E_T^{plus}, E_{ref} and E_T^{min}, and α_C from E_C and E_{ref}. Details can be found in section 2.3.

For the experiments with constant relative humidity the scaling α_T remains relatively constant for each percentile, Scaling derived from the positive perturbation α_T^{plus} ($\sim$15% per degree) and the negative perturbation α_T^{min} ($\sim$10% per degree) show larger variations. Although the highest percentiles of E_C show a scaling strength similar to the E_T^{plus} perturbation, the lower percentiles of the E_C experiment show a decrease with respect to E_{ref}. Recall (figure 5(a)) that the lower E_C percentiles are very similar to those in the E_T^{plus} experiment when we consider only data with precipitation of at least 1 mm h^{-1}. This suggests that the reduction of the lower percentiles obtained with the climate change perturbation is primarily related to the changes in precipitation frequency, defined by precipitation amounts larger than 1 mm h^{-1}.

4. Behavior of all cases

Up to this point, we have only analyzed an individual case. However, the results of individual cases can easily contain random components due to the chaotic, unpredictable behavior of convective clouds at small scales, which might be reflected

in the distribution of precipitation extremes. For example, in some cases (e.g. case 3, supplementary material available at stacks.iop.org/ERL/9/014003/mmedia), the distribution of the reference experiment shows a disproportional increase in precipitation intensity for the highest percentile range. As a consequence, the computed sensitivity to a temperature increase (α_T^{plus} and α_C) is considerably reduced, while the sensitivity to a temperature decrease (α_T^{min}) is enlarged. Therefore, this section concentrates on the aggregated behavior of cases. The first part focusses on the average behavior of the single cases, and in the second part we compute the statistics for the pooled data. Results of each case separately can be found in the supplementary material available at stacks.iop.org/ERL/9/014003/mmedia.

4.1. Average behavior

Table 3 provides an overview of the averaged change in the area of hourly precipitation. The area with a precipitation threshold of 1 mm h^{-1} increases with temperature by approximately 4% per degree for the idealized perturbations. However, this trend is reversed for the climate perturbation, where we find a decrease in the precipitating area of approximately 5% per degree. Both the climate and idealized perturbations show a substantial increase in the averaged precipitating area for the highest threshold of 30 mm h^{-1}.

Most of the individual cases correspond with this averaged behavior. However, case 10 stands out, with the 30 mm h^{-1} area decreasing for both increasing and decreasing temperatures. Coincidentally, this case has the lowest relative humidity and highest temperature of all cases considered. Furthermore, the large scale pattern of precipitation varies for the four experiments (see supplementary material available at stacks.iop.org/ERL/9/014003/mmedia), suggesting that the
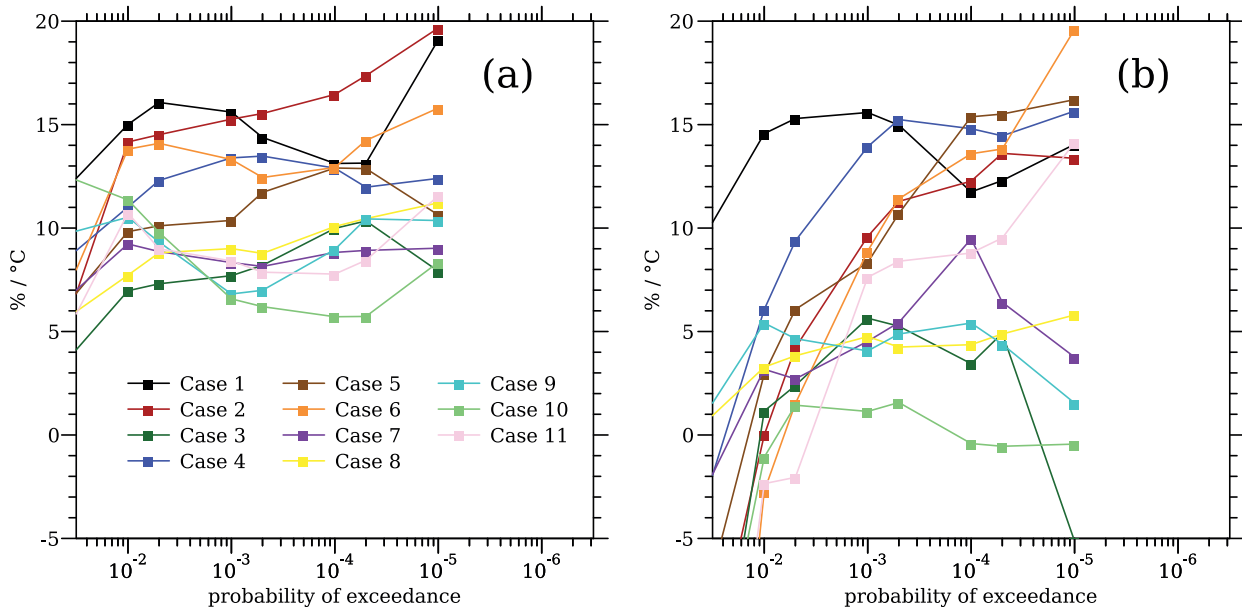
Figure 6. (a) Precipitation scaling under constant relative humidity α_T; (b) precipitation scaling including lapse rate and relative humidity changes α_C.

Table 3. The change in area with hourly precipitation exceeding a threshold of 1, 10, and 30 mm h^{-1}.

Experiment	1 mm h^{-1}(% per degree)	10 mm h^{-1}(% per degree)	30 mm h^{-1}(% per degree)
E_T^{min}	−4	−18	−31
E_T^{plus}	4	27	38
E_C	−5	17	27

experimental setup is not very suitable for this case. Despite this, we have chosen to retain this experiment in the average statistics.

The temperature dependencies of hourly precipitation intensity derived from the idealized perturbations (α_T) and from the climate change perturbation (α_C) are shown in figure 6. There is a large spread in dependency, with cases scaling in the range of close to 0 up to 17% per degree. A number of cases, 3 and 7–10, show comparatively low scaling for the climate change perturbation. Averaging the sensitivities of all cases gives a dependency of $\alpha_T = 11.2\%$ per degree for the idealized perturbation, and $\alpha_C = 8.5\%$ per degree for the climate perturbation. When we compare α_C to the positive temperature perturbation α_T^{plus}, which gives 10.5% per degree, the sensitivity to a climate change perturbation is 2% smaller than to the idealized perturbation. Leaving the suspicious case 10 out of the statistics results in approximately 1% per degree higher sensitivities for α_T^{plus} and α_C, and little change in the others (not shown).

Singleton and Toumi (2013) suggest that the propagation speed of convective systems might depend on the temperature perturbation, which could affect the scaling for longer accumulation periods. This factor is not likely to play a key role here, because the time evolution of intensity and the spatial fields of accumulated precipitation of the different perturbed experiments experiment are similar. Furthermore, we have investigated instantaneous rain rates, which are available once per hour in the current model setup and are derived from one time step (60 s). The resulting scaling relations are shown in figure 7. Although individual cases show an increase in sensitivity, overall the results are comparable to those based on the hourly data.

4.2. Statistics based on combined cases

In this section, we analyze the statistics of all cases combined into one large 11 day event. The probability of exceedance of hourly precipitation is shown in figure 8(a) for the reference and perturbed experiments. Compared to the results based on single days, the distributions are smoother with a clear exponential tail (that is, linear lines in the plots). As a result, the derived temperature dependencies behave more smoothly, with less variation over the different percentiles (figure 8(b)). The rates of increase derived for the idealized perturbations, α_T, α_T^{min}, and α_T^{plus}, are now very similar. For moderate extreme events (99.9 percentile, or POE of 10^{-3}) the dependency is close to 11% per degree, and increases to 12–13% per degree for the tail of the distribution with a POE of 10^{-5} and smaller. Note that here, a POE of 10^{-5} corresponds to approximately 300 events of hourly grid box precipitation.
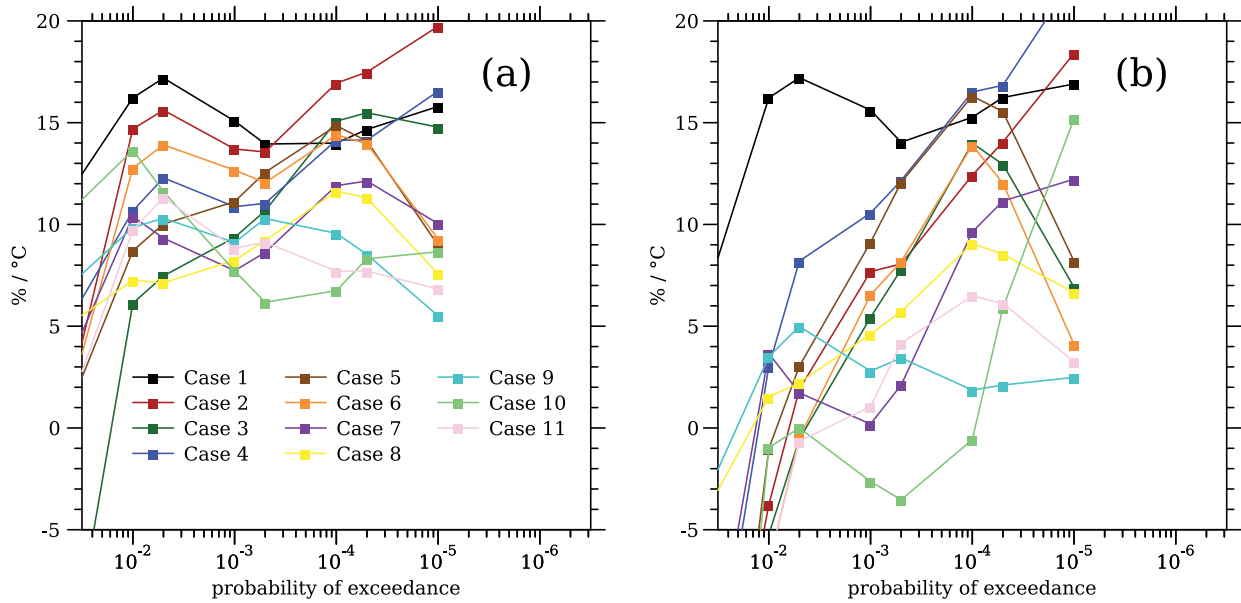
Figure 7. Scaling of instantaneous precipitation rates of (a) α_T and (b) α_C (colors are the same as in figure 6). Due to model configuration, rain rates were only available once per hour.
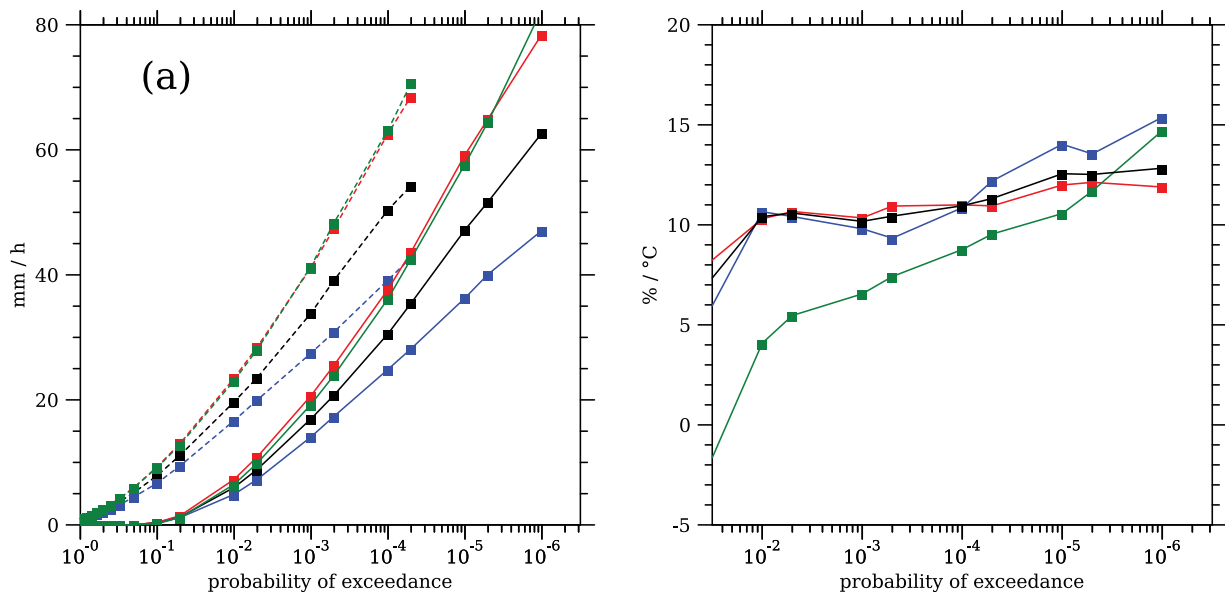

Figure 8. Precipitation scaling for the combined cases. Colors and lines are the same as in figure 5.

With an increase of around 7% per degree, the moderate extremes of the climate change perturbation show a weaker sensitivity than the idealized perturbation (POE of 10^{-3} in figure 5). These events are likely to be affected most by the reduction in relative humidity and the change in lapse rate. However, for the more extreme events with a POE range between 10^{-4} and 10^{-5}, the difference amounts to approximately 2% per degree. This corresponds with the averaged results over the cases. For the most extreme events the difference between idealized and climate change perturbation even appears to vanish.

It has been shown that cases 3 and 7–10 have a rather low sensitivity α_C to the climate perturbation. These cases

also have the lowest sensitivity to a temperature increase using the idealized perturbation (see table 4). Remarkably, the same cases display a large sensitivity to a temperature decrease, suggesting there might be a limit on the increase in intensity for these cases. However, poor statistics as discussed in the beginning of this section could also be a reason. To investigate this further, we split the data set into two groups depending on α_C: a group containing these weakly scaling cases (3 and 7–10) and a group containing the remaining cases with stronger scaling. The scaling factors derived from these two groups are shown in figure 9 and the full distribution is plotted in figure 10.

The 'strong scaling' combination has the same characteristics as the combination of all cases, with a slightly larger
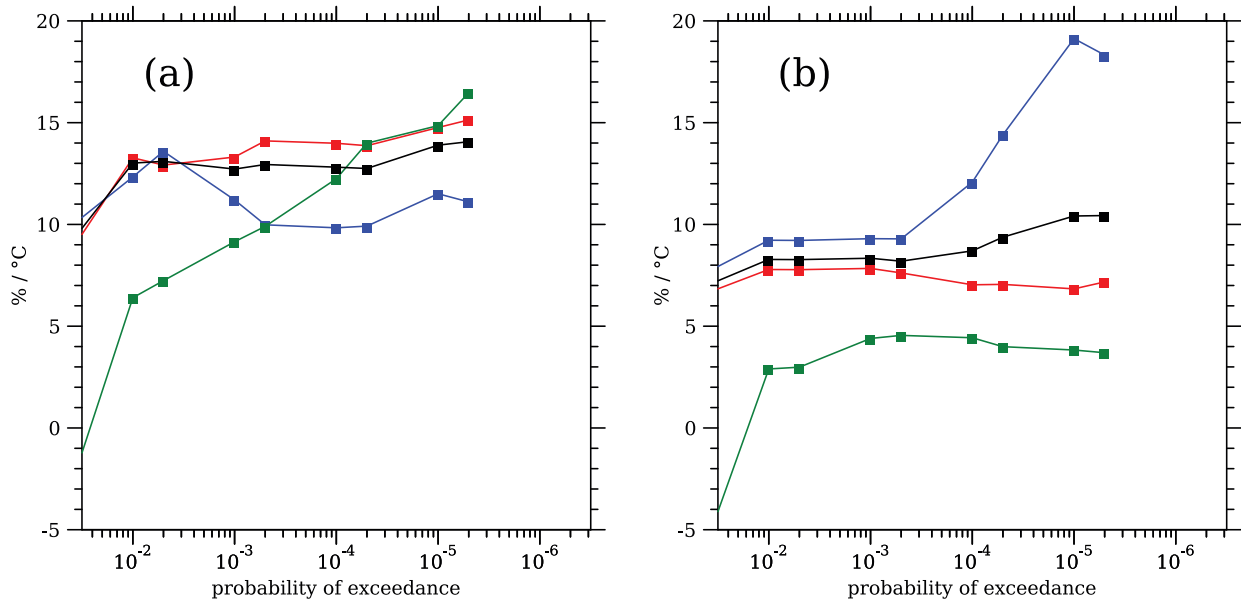
Figure 9. Precipitation scaling for two different combinations of the cases. (a) Combination of cases showing super-CC scaling (1, 2, 4–6, 11); (b) combination of cases which scale with CC or weaker (3, 7–10). Colors are the same as figure 5.

Figure 10. Probability of exceedance for two different combinations of the cases. (a) Combination of cases showing super-CC scaling (1, 2, 4-6, 11); (b) combination of cases which scale with CC or weaker (3, 7-10). Colors are the same as figure 5.
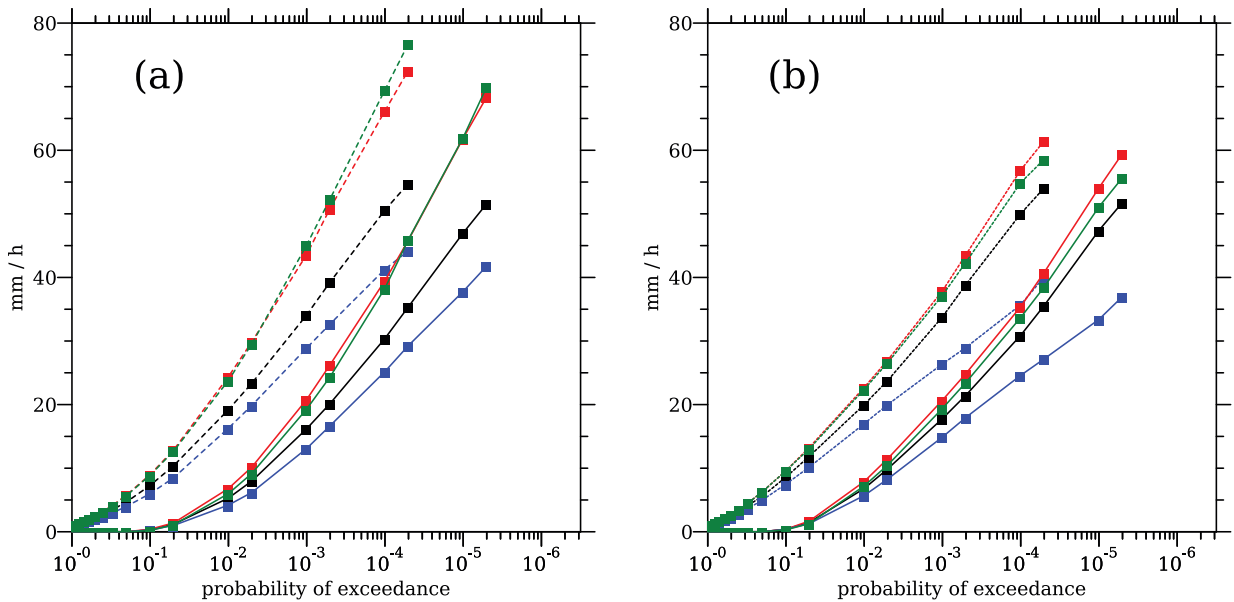
α_T of 13% per degree. The scaling is also less dependent on the percentiles. In the 'weak scaling' combination, results differ more strongly from the full set. Both positive perturbations show rather small increases in precipitation intensity compared to the reference, for α_C typically 4% per degree and α_T^{plus} typically 7% per degree. However, the sensitivity to temperature decrease is much larger, with values of α_T^{min} peaking above 15% per degree. The large difference between the scaling derived from a temperature decrease and a temperature increase, as well as the very high sensitivity to a temperature decrease suggest that random errors could play a role. Indeed, inspecting the distributions it is shown that the reference simulations bend

upward in the tail of the distribution, whereas the 2° colder simulations bend downward.

On the other hand, we do believe that physical effects might explain the difference between the two groups. First, limitations due to moisture supply to the convective clouds might play a role. Scaling in excess of the CC relation can only be sustained if sufficient moisture is supplied to the convective clouds through the mesoscale atmospheric motions. This is clear from the fact that the precipitation rate is large compared to the amount of moisture contained in an atmospheric column. This hypothesis is partly supported by the finding that the climate perturbation gives a systematically

Table 4. Scaling of precipitation with temperature for the combined cases. Precipitation scaling is the average of the scaling for the 99.9, 99.99, and 99.999 percentile. See table B1 of the supplementary material for a discussion of the convergence of the higher percentiles.

Case	$\alpha_T^{\min}$ (% per degree)	α_T^{plus} (% per degree)	α_T (% per degree)	α_C (% per degree)
1	14	17	16	14
2	14	18	17	12
3	19	4	9	1
4	12	13	13	15
5	11	11	11	13
6	10	15	14	14
7	11	8	9	6
8	15	8	10	5
9	12	7	9	4
10	12	4	7	0
11	6	11	9	10
Average	12.3	10.5	11.2	8.5
Combined cases				
All (1-11)	12	11	11	9
Strong scaling (1, 2, 4–6, 11)	11	14	13	12
Weak scaling (3, 7–10)	14	7	9	4

lower sensitivity compared to the idealized perturbation in the weak scaling group, whereas the difference vanishes for the tail of the distribution in the strong scaling group. Furthermore, limitations on the production of rain through the cloud microphysics might be of influence. There is some support for this in the behavior of instantaneous precipitation rate. For the highest rates, peaking at 120 mm h^{-1} the sensitivity to temperature appears to be smaller compared to the sensitivity at lower rates (see also supplementary material available at stacks.iop.org/ERL/9/014003/mmedia).

5. Conclusions

In this letter, the temperature dependency of extremes in (sub)hourly precipitation is investigated for 11 cases for the Netherlands using the convective permitting mesoscale model Harmonie, by perturbing the initial conditions of the atmosphere. To this end, we have applied two idealized perturbations and a more realistic perturbation derived from a long climate change simulation to the reference experiment. The two idealized perturbations consist of a constant positive and negative 2° temperature perturbation with height and unchanged relative humidity. The climate perturbation is characterized by a small decrease in relative humidity, a stronger temperature increase in the lower part of the atmosphere, and increase in stability higher up in the atmosphere. The increase in dew point temperature near the surface, which measures the absolute humidity and which we consider most relevant (Lenderink and van Meijgaard 2010, Lenderink *et al* 2011), is approximately 2° in this climate change perturbation, and is therefore the same as in the idealized perturbation.

The idealized perturbations show an increase of extreme hourly precipitation of 11% per degree, averaged over all cases and a number of extreme percentiles. The precipitating area increases with approximately 4% per degree. With a decrease of approximately 5% per degree, this effect on the precipitating area is reversed for the climate perturbation. At the same time, hourly precipitation extremes of the climate

perturbation increase at a rate of 9% per degree. This slightly lower rate of increase with respect to the idealized perturbation experiments is primarily caused by the lower percentiles, which are strongly affected by the decrease in area with precipitation. By combining all cases into one data set of 11 days the same dependencies are found. In addition, for the most extreme events a convergence between the results of the idealized and climate change perturbation appears to occur at a rate of 11–14% per degree (see figure 8). This is close to a temperature dependency of approximately 14% per degree which is derived from observations (Loriaux *et al* 2013, Berg *et al* 2013).

Results for the separate cases, however, show a wide range in sensitivity, between 7 and 17% per degree for the idealized perturbation (combined positive and negative perturbation) and 0 and 15% per degree for the climate change perturbation. The spread in part could be explained by the randomness introduced by the chaotic (unpredictable) behavior of these showers at small scales. However, a number of cases (5 out of 11) appear to display a lower sensitivity to a temperature increase than a temperature decrease, which could be an indication of a break down in precipitation scaling at high temperatures. We speculate that this might be related to the cloud micro-physics or to limitations in moisture supply to the cloud by the atmospheric circulation on the mesoscale. These aspects clearly deserve more research.

Acknowledgment

Appendix. Parametrized profiles

In this section we will discus the perturbation method, and the consequences of the applied perturbations in terms of large scale dynamics. The atmospheric boundaries and initial conditions are given at (hybrid) pressure levels, and contain

temperature (T), horizontal wind components (u, v), and humidity (q), and are assumed to be in hydrostatic equilibrium. The perturbation is applied as follows. First, we calculate the relative humidity (RH). Then we apply the follow perturbations to T and RH:

$$T \rightarrow T' = T + \Delta T(p) \tag{A.1}$$

$$\text{RH} \rightarrow \text{RH}' = \text{RH} + \Delta\text{RH}(p). \tag{A.2}$$

Using the perturbed temperature and relative humidity we recalculate the humidity to obtain a new set of boundaries (T', q', u, v). It is important that the perturbations do not destabilize the atmosphere by creating an inconsistent set of boundary conditions, and here we will briefly discuss two possible sources of instability: hydrostatic equilibrium and thermal winds.

The geopotential height is calculated using the hydrostatic equation and the surface pressure, so the hydrostatic equilibrium is enforced. This also raises the geopotential height of the pressures levels: The moist air close to the surface is lighter so a pressure drop δp corresponds to a thicker layer δz. However, the increase of tropopause height in pressure levels is missed.

A second source of instability is an inconsistency between the temperature and wind profiles, linked via the thermal wind equation. Thermal winds are a consequence of a horizontal temperature gradient:

$$\vec{v}_T = \frac{R}{f}\ln\frac{p_0}{p_1}\vec{k} \times \nabla_p T_v \tag{A.3}$$

where R is the gas constant for dry air, f is the Coriolis parameter, p_0 and p_1 are two pressure levels, and T_v is the virtual temperature. The changes in thermal wind are negligible as long as the derivative of ΔT_v is small:

$$\Delta\vec{v}_T = \vec{v}_{T'} - \vec{v}_T = \frac{R}{f}\ln\frac{p_0}{p_1}\vec{k} \times \nabla_p \Delta T_v. \tag{A.4}$$

The largest contribution to $\vec{v}_T$ is from the temperature. When we ignore the moisture we find $\nabla_p\Delta T_v \approx \nabla_p\Delta T(p) = 0$, the thermal winds are unchanged. Next we consider the moisture contribution to the thermal wind. This is, apart from some constants:

$$\vec{v}_v \sim \nabla_p(T_v - T) \sim \nabla_p qT. \tag{A.5}$$

Assuming a CC scaling for the saturation humidity (q_{sat}) of 7% per degree, we can use (A.2) to write the perturbed specific humidity as:

$$
\begin{aligned}
q \rightarrow q' &= (\text{RH} + \Delta\text{RH})q_{sat}(T + \Delta T) \\
&\approx 1.07^{\Delta T}\left(1 + \frac{\Delta\text{RH}}{\text{RH}}\right)q.
\end{aligned} \tag{A.6}
$$

Applying perturbations (A.1) and (A.6) to (A.5) gives:

$$\vec{v}_v' \approx (1.07)^{\Delta T}\left(1 + \frac{\Delta\text{RH}}{\text{RH}}\right)\vec{v}_v \tag{A.7}$$

where we used the approximation that the change in temperature is small compared to the temperature. For realistic profiles the moisture contribution, which is itself small, changes about 10–30%.

We conclude that the atmosphere remains consistent under perturbation (A.1) and (A.2). Also, the response of the atmospheric profile to climate change as found by GCMs can be reasonably described by this transformation.

References

Allen M R and Ingram W J 2002 *Nature* **419** 224–32

Benard P, Vivoda J, Masek J, Smolikova P, Yessad K, Smith C, Brozkova R and Geleyn J F 2010 *Q. J. Roy. Meteor. Soc.* **136** 155–69

Berg P, Moseley C and Haerter J O 2013 *Nat. Geosci.* **6** 181–5

Böing S J, Siebesma A P, Korpershoek J D and Jonker H J J 2012 *Geophys. Res. Lett.* **39** 20

Bubnová R, Hello G, Bénard P and Geleyn J-F 1995 *Mon. Weather Rev.* **123** 515–35

Colman R 2004 *Geophys. Res. Lett.* **31** L21109

Dee D P *et al* 2011 *Q. J. R. Meteorol. Soc.* **137** 553–97

Haerter J O and Berg P 2009 *Nature Geosci.* **2** 372–3

Haylock M R, Hofstra N, Klein Tank A M G, Klok E J, Jones P D and New M 2008 *J. Geophys. Res.: Atmos.* **113** D20119

Hazeleger W *et al* 2012 *Clim. Dyn.* **39** 2611–29

Held I M and Soden B J 2006 *J. Clim.* **19** 5686–99

Kharin V V, Zwiers F W, Zhang X and Hegerl G C 2007 *J. Clim.* **20** 1419–44

Kharin V V, Zwiers FW, Zhang X and Wehner M 2013 *Clim. Change* **119** 345–57

Lenderink G, Mok H Y, Lee T C and van Oldenborgh G J 2011 *Hydrol. Earth Syst. Sci.* **15** 3033–41

Lenderink G and van Meijgaard E 2008 *Nature Geosci.* **1** 511–4

Lenderink G and van Meijgaard E 2010 *Environ. Res. Lett.* **5** 025208

Loriaux J M, Lenderink G, de Roode S R and Siebesma A P 2013 *J. Atmos. Sci.* **70** 3641–55

Min S K, Zhang X, Zwiers F W and Hegerl G C 2011 *Nature* **470** 378–81

Muller C J 2013 *J. Clim.* **26** 5028–43

Muller C J and O'Gorman P A 2011 *Nature Clim. Change* **1** 266–71

Muller C J, O'Gorman P A and Back L E 2011 *J. Clim.* **24** 2784–800

O'Gorman P A 2012 *Nature Geosci.* **5** 697–700

O'Gorman P A and Muller C J 2010 *Environ. Res. Lett.* **5** 025207

O'Gorman P A and Schneider T 2009a *J. Clim.* **22** 5676–85

O'Gorman P A and Schneider T 2009b *Proc. Natl Acad. Sci. USA* **106** 14773–7

Pall P, Allen M R and Stone D A 2006 *Clim. Dyn.* **28** 351–63

Romps D M 2011 *J. Atmos. Sci.* **68** 123–38

Seity Y, Brousseau P, Malardel S, Hello G, Benard P, Bouttier F, Lac C and Masson V 2011 *Mon. Weather Rev.* **139** 976–91

Sherwood S C, Ingram W, Tsushima Y, Satoh M, Roberts M, Vidale P L and O'Gorman P A 2010 *J. Geophys. Res. Atmos.* **115**

Singleton A and Toumi R 2013 *Q. J. R. Meteorl. Soc.* **139** 334–9

Soden B J and Held I M 2006 *J. Clim.* **19** 3354–60

Sugiyama M, Shiogama H and Emori S 2010 *Proc. Natl Acad. Sci.* **107** 571–5

Taylor K E, Stouffer R J and Meehl G A 2012 *Bull. Am. Meteorol. Soc.* **93** 485–98

Trenberth K E, Dai A, Rasmussen R M and Parsons D B 2003 *Bull. Am. Meteorol. Soc.* **84** 1205

van Meijgaard E, van Ulft L, van de Berg W, Bosveld F, van den Hurk B, Lenderink G and Siebesma A 2008 *KNMI Technical Report*, 302 http://www.knmi.nl/bibliotheek/knmipubTR/TR302.pdf

Willett K M, Jones P D, Thorne P W and Gillett N P 2010 *Environmen. Res. Lett.* **5** 025210